EPJ Plus

EPJ.org
your physics journal

Eur. Phys. J. Plus (2019) **134**: 13 DOI 10.1140/epjp/i2019-12431-7

Thermal radiation effect on the flow field and heat transfer of Co_3O_4-diamond/EG hybrid nanofluid using experimental data: A numerical study

Ali Akbar Abbasian Arani, Farhad Monfaredi, Alireza Aghaei, Masoud Afrand, Ali J. Chamkha and Hesamoddin Emami

Società Italiana di Fisica

Springer

Eur. Phys. J. Plus (2019) **134**: 13
DOI 10.1140/epjp/i2019-12431-7

THE EUROPEAN PHYSICAL JOURNAL PLUS

Regular Article

Thermal radiation effect on the flow field and heat transfer of Co_3O_4-diamond/EG hybrid nanofluid using experimental data: A numerical study

Ali Akbar Abbasian Arani[1], Farhad Monfaredi[1], Alireza Aghaei[2,a], Masoud Afrand[3], Ali J. Chamkha[4,5], and Hesamoddin Emami[1]

[1] Department of Mechanical Engineering, University of Kashan, Kashan, Iran
[2] Young Researchers and Elite Club, Arak Branch, Islamic Azad University, Arak, Iran
[3] Department of Mechanical Engineering, Najafabad Branch, Islamic Azad University, Najafabad, Iran
[4] Mechanical Engineering Department, Prince Sultan Endowment for Energy and Environment, Prince Mohammad Bin Fahd University, Al-Khobar 31952, Saudi Arabia
[5] RAK Research and Innovation Center, American University of Ras Al Khaimah, P.O. Box 10021, Ras Al Khaimah, United Arab Emirates

Received: 21 June 2018 / Revised: 21 October 2018
Published online: 10 January 2019

Abstract. In this study, the impact of thermal radiation on fluid flow and heat transfer within a square enclosure filled with ethylene glycol-Co_3O_4-diamond hybrid nanofluid on the basis of experimental data is investigated. The governing equations are being solved by employing the finite volume method and the SIMPLER algorithm. In investigating this problem, the Rayleigh number is taken from $Ra = 10^3$ to $Ra = 10^5$ and the volume fraction of nanoparticles in the range from 0.0 to 0.075 percent and the values from 0 to 2 are considered for the radiation parameter. It is observed from the results that in all the considered volume fractions, the average Nusselt number is increased by increasing the value of the radiation parameter. In all of the considered values for Ra and the volume fractions, the most relevant enhancement in the average Nusselt number corresponding to the enhancement of the radiation parameter is 200.25 percent which occurs in $Ra = 10^5$ while the volume fraction is 0.075. In all volume fractions investigated, the maximum value of the stream function is increased by increasing the value of the radiation parameter. For all Rayleigh numbers in each of the investigated values of the radiation parameter, the maximum value of the stream function decreases by increasing the volume fraction of nanoparticles. The results of this study reveal that the effect of the thermal radiation in high Rayleigh numbers is not considerable.

1 Introduction

Hybrid nanofluids are a new class of nanofluids engineered by dispersing more than one nanofluid for the purpose of achieving different thermophysical characteristics as compared to nanofluid containing single nanoparticles. Hybrid nanofluids are produced by two methods:

A) Dispersing two different nano particles in the base fluid.

B) Dispersing nanoparticles stock together (composite) in the base fluid.

Natural convection heat transfer exists in different areas of industrial sectors and is used in solar thermal collectors, air conditioning, cooling of electronic components, etc. Using nanofluids is a new passive method for increasing heat transfer. Khanafer *et al.* [1] investigated the impact of using nanofluids within an enclosure on increasing heat transfer. They employed different models to study the features of nanofluids. They observed that in each Grashof number, heat transfer increases by increasing the volume fraction of nanoparticles. In a numerical study, Ho *et al.* [2] employed a finite

[a] e-mail: a-aghaei@iau-arak.ac.ir (corresponding author)

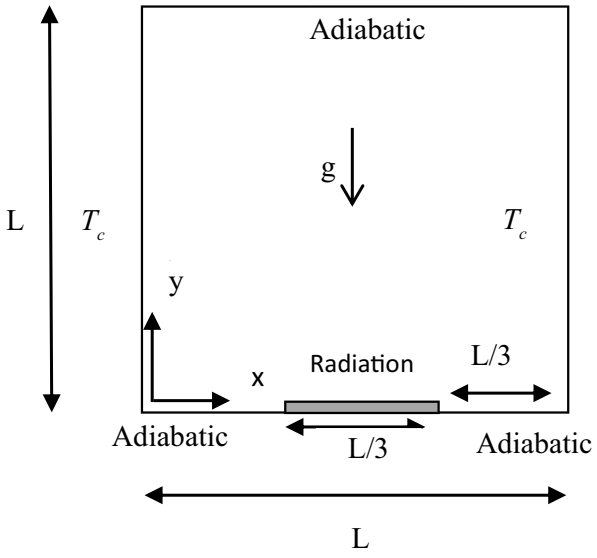

Fig. 1. Schematic of the enclosure with the boundary conditions.

volume fraction method to investigate free convection heat transfer of a square enclosure with insulated horizontal and cold/hot vertical walls filled with water-Al_2O_3. Based on their investigation, employing different models for viscosity can predict different values for the Nusselt number. Oztop and Abu-Nada [3] studied fluid flow and natural convection heat transfer within a heated enclosure filled with a variable amount of nanofluids and nanoparticles. They concluded that using nanofluids in low aspect ratio has more effect on heat transfer enhancement in comparison to high aspect ratio. Öğüt [4] investigated natural convection of different water-based nanofluids within an inclined enclosure considering partial heating. Based on his investigations convection heat transfer increases by increasing the nanoparticle's volume fraction; additionally nanoparticles like Ag and Cu could increase heat transfer. Jahanshahi *et al.* [5] conducted numerical and experimental study by employing the finite volume method to investigate free convection heat transfer within a square enclosure filled with water-SiO_2. The results also indicate that the average Nusselt number increases by increasing the volume fraction of nano-particles in all considered Rayleigh number range. Saleh *et al.* [6] conducted a numerical study of natural convection heat transfer in a trapezoidal enclosure filled with Cu-water and Al_2O_3-water nanofluid and the results indicate that he maximum average Nusselt number occurs in the highest volume fraction for Cu nanoparticles (0.05) in the maximum inclination angle of side walls with the vertical direction. Aminossadati and Ghasemi [7] conducted a numerical investigation on natural convection of water-CuO nanofluid in variable Grashof number and volume fractions. Based on the results, the average Nusselt number increases by increasing the Rayleigh number and the volume fraction of the nanoparticles. Fluid flow and heat transfer caused by natural convection of Cu-water within a c-shape enclosure were studied by Mahmoodi and Hashemi [8]; they concluded that the average Nusselt number increases by increasing the Rayleigh number and the volume fraction of the nanoparticles. Valipour *et al.* [9] in 2017 investigated the impact of the radiation parameter on the heat transfer of nanofluids between parallel plates considering a magnetic field effect. Recently, new and interesting new studies have been carried out on the behaviour of nanofluids in related fields [10–15].

The purpose of this work is to employ experimental data to study the effect of thermal radiation on flow field and heat transfer within a rectangular enclosure filled with ethylene glycol-Co_3O_4-diamond hybrid nanofluid. The results of this study are obtained for the parametric range of 10^4 to 10^5 for the Rayleigh number and (0–0.075) percent of the nanoparticle volume fraction and (0–2) for the radiation parameter.

2 Problem formulation and boundary condition

The rectangular enclosure and boundary conditions are depicted in fig. 1. The length of enclosure is denoted by L and the bottom wall is elevated in the middle part which includes also thermal radiation and in the other parts the wall is insulated. The vertical walls and top wall of the enclosure are cold and insulated, respectively, and there is a two-dimensional, steady-state and laminar fluid flow.

The thermophysical properties of ethylene glycol as a base fluid diamond and Co_3O_4 nanoparticles are presented in table 1 [16–18].

Table 1. Thermophysical properties of base fluid and nanoparticles [16–18].

Physical properties	β (K^{-1})	k (W/m K)	c_p (J/kg K)	ρ (kg/m^3)	μ (kg/m s)
EG	27.61×10^{-5}	0.252	2415	1114.4	157×10^{-5}
ND	10^{-4}	1000	516	3100	–
Co_3O_4	1.85×10^{-5}	99.2	421	8862	–

The continuity, x- and y-components of the momentum, and energy equations for the two-dimensional steady and laminar flow of the nanofluid are given by [2]

$$\frac{\partial u}{\partial x} + \frac{\partial v}{\partial y} = 0, \tag{1}$$

$$u\frac{\partial u}{\partial x} + v\frac{\partial u}{\partial y} = -\frac{1}{\rho_{nf}}\frac{\partial p}{\partial x} + \frac{1}{\rho_{nf}}\left[\frac{\partial}{\partial x}\left(\mu_{nf}\frac{\partial u}{\partial x}\right) + \frac{\partial}{\partial y}\left(\mu_{nf}\frac{\partial u}{\partial y}\right)\right], \tag{2}$$

$$u\frac{\partial v}{\partial x} + v\frac{\partial v}{\partial y} = -\frac{1}{\rho_{nf}}\frac{\partial p}{\partial y} + \frac{1}{\rho_{nf}}\left[\frac{\partial}{\partial x}\left(\mu_{nf}\frac{\partial v}{\partial x}\right) + \frac{\partial}{\partial y}\left(\mu_{nf}\frac{\partial v}{\partial y}\right)\right] + \frac{(\rho\beta)_{nf}}{\rho_{nf}}g(T - T_c) \tag{3}$$

and

$$u\frac{\partial T}{\partial x} + v\frac{\partial T}{\partial y} = \frac{1}{(\rho c_p)_{nf}}\left[\frac{\partial}{\partial x}\left(k_{nf}\frac{\partial T}{\partial x}\right) + \frac{\partial}{\partial y}\left(k_{nf}\frac{\partial T}{\partial y}\right)\right]. \tag{4}$$

In order to cast the governing equation into a dimensionless form, the following dimensionless variables are introduced [19]:

$$X = \frac{x}{L}, \qquad Y = \frac{y}{L}, \qquad \theta = \frac{T - T_c}{T_h - T_c}, \qquad U, V = \frac{(u, v)L}{\alpha_f}, \qquad R_d = \frac{4\sigma_r T_c^3}{kk^*}, \qquad Pr = \frac{\nu_f}{\alpha_f}. \tag{5}$$

The dimensionless governing equations are given by:

$$\frac{\partial U}{\partial X} + \frac{\partial V}{\partial Y} = 0, \tag{6}$$

$$U\frac{\partial U}{\partial X} + V\frac{\partial U}{\partial Y} = -\frac{\partial P}{\partial X} + \frac{1}{\rho_{nf}\alpha_f}\frac{\partial}{\partial X}\left(\mu_{nf}\frac{\partial U}{\partial X}\right) + \frac{\partial}{\partial Y}\left(\mu_{nf}\frac{\partial U}{\partial Y}\right), \tag{7}$$

$$U\frac{\partial V}{\partial X} + V\frac{\partial V}{\partial Y} = -\frac{\partial P}{\partial Y} + \frac{1}{\rho_{nf}\alpha_f}\left[\frac{\partial}{\partial X}\left(\mu_{nf}\frac{\partial U}{\partial X}\right) + \frac{\partial}{\partial Y}\left(\mu_{nf}\frac{\partial U}{\partial Y}\right)\right] + \frac{(\rho\beta)_{nf}}{\rho_{nf}\beta_f}RaPr\theta, \tag{8}$$

$$u\frac{\partial T}{\partial x} + v\frac{\partial T}{\partial y} = \frac{1}{(\rho c_p)_{nf}}\left(1 + \frac{4R_d}{3}\right)\left[\frac{\partial}{\partial x}\left(k_{nf}\frac{\partial T}{\partial x}\right) + \frac{\partial}{\partial y}\left(k_{nf}\frac{\partial T}{\partial y}\right)\right]. \tag{9}$$

The dimensionless boundary conditions are given by

$$\begin{aligned} &U = V = 0, \quad \theta = 0 \quad \text{On the vertical walls of the enclosure.} \\ &U = V = 0, \quad \frac{\partial\theta}{\partial Y} = 0 \quad \text{On the top and bottom walls except the radiation area} \\ &\frac{\partial\theta}{\partial Y} = 1 \quad \text{Radiation area.} \end{aligned} \tag{10}$$

3 Nanofluid properties

The nanofluid properties including density, heat capacity, thermal expansion coefficient and thermal diffusivity are obtained from the following relations, respectively:

$$\rho_{nf} = (1 - \varphi)\rho_f + \varphi_1\rho_{s1} + \varphi_2\rho_{s2}, \tag{11}$$

$$(\rho c_p)_{nf} = (1 - \varphi)(\rho c_p)_f + \varphi_1(\rho c_p)_{s1} + \varphi_2(\rho c_p)_{s2}, \tag{12}$$

$$(\rho\beta)_{nf} = (1 - \varphi)(\rho\beta)_f + \varphi_1(\rho\beta)_{s1} + \varphi_2(\rho\beta)_{s2}, \tag{13}$$

$$\alpha_{nf} = \frac{k_{nf}}{(\rho c_p)}. \tag{14}$$

Implementing the experimental study of Sundar *et al.* [20], the viscosity and thermal conductivity of hybrid nanofluids prepared with ethylene glycol-Co_3O_4-diamond are obtained from the following relations:

$$\frac{k_{nf}}{k_f} = 0.99781(1+\varphi)^{0.6556}, \tag{15}$$

$$\frac{\mu_{nf}}{\mu_f} = 0.9595(1+\varphi)^{2.399}. \tag{16}$$

The convection heat transfer coefficient is given by

$$h_{nf} = \frac{q}{T_h - T_c}\,. \tag{17}$$

The Nusselt number whose characteristic length is commensurate with the length of enclosure is defined as

$$Nu = \frac{h_{nf}L}{k_f}\,. \tag{18}$$

The heat flux per unit on walls is defined as

$$q = -k_{nf}\frac{T_h - T_c}{L}\frac{\partial\theta}{\partial n}\,. \tag{19}$$

Substituting eq. (17) and (19) into (18) and rearranging gives the Nusselt number as:

$$Nu = \left(\frac{k_{nf}}{k_f}\right)\left(1 + \frac{4}{3}Rd\left(\frac{k_{nf}}{k_f}\right)^{-1}\right)\frac{\partial\theta}{\partial Y}\,. \tag{20}$$

The average Nusselt number on hot walls is obtained from following relation:

$$Nu_{avg} = \frac{1}{L/3}\int_{L/3}^{2L/3} Nu\mathrm{d}X. \tag{21}$$

4 Numerical simulation

The finite volume method and the SIMPLER algorithm are employed to solve the governing mass, momentum, and energy equations numerically. This method is suitable in light of previous works [21–28]. The first step in discretizing the governing equations is to generate a finite difference mesh in the computational domain. Subsequently, a control volume is generated around each node of the mesh. The governing equations are then integrated over each control volume. Integration of the diffusion terms, *i.e.*, over the control volume results in the products of the nanofluid viscosity and its thermal conductivity with the first derivatives of the velocity components and the temperature with respect to the space variables on the faces of the control volume. To compute these products while using the variable-property models, the thermal conductivity and the viscosity of the nanofluid on each face of the control volume are evaluated at the average temperature of the surrounding nodes of that face. Moreover, the derivatives of the dependent variables on the faces of the control volume are replaced by the finite difference expressions written in terms of the nodal values of the dependent variables. The diffusion terms are replaced using a second-order central difference scheme; while a hybrid scheme, *i.e.* a combination of upwind and central difference schemes, is employed for the convective terms in order to stabilize the solutions for the convection-dominated cases. Performing the same procedure for all of the control volumes in the computational domain yields a nonlinear system of algebraic equations with the nodal values of the dependent variables as the unknowns. The nonlinear system of discretized equations is subsequently solved iteratively yielding the velocity, the pressure, and the temperature at the nodal points. An under relaxation scheme is employed to obtain converged solutions.

5 Validation

The numerical simulations of natural convection [7] are used to evaluate the computing result and the results of the simulation are given in table 2. As is observed from table 2, very little difference exists between the result of the simulation obtained by the present numerical method and the result of Aminossadati and Ghasemi [7] (considered as error).

Table 2. Comparisons between the average Nusselt number and the results of [7].

Ra	φ	Nu_{avg}	
		Present work	[7]
10^3	0	3.34	3.37
	0.02	3.75	3.78
	0.04	3.90	3.92
10^4	0	3.40	3.43
	0.02	3.81	3.84
	0.04	3.96	3.99
10^5	0	4.06	4.07
	0.02	4.46	4.48
	0.04	4.60	4.61

Table 3. The average Nusselt number at $\varphi = 0.075$ and $Ra = 10^5$, $Rd = 1$.

Number of grid points	Nu_{avg}
81×41	4.81
101×51	5.19
121×61	5.42
141×71	5.45

In order to determine a proper grid for the grid-independent result, the average Nusselt number of water-Al_2O_3 nanofluid for grid with variable node number is compared in table 3. It is concluded from the average Nusselt number observed that the grid having 121×61 nodes is sufficiently adequate and all the following results are obtained by employing this grid to perform the needed calculation.

The convergence criteria are obtained from the following relation:

$$\text{Error} = \frac{\sum_{i=1}^{M}\sum_{j=1}^{N}|\zeta_{ij}^{k+1} - \zeta_{ij}^{k}|}{\sum_{i=1}^{M}\sum_{j=1}^{N}|\zeta_{ij}^{k+1}|} \leq 10^{-7}. \tag{22}$$

6 Results and discussion

The streamlines and isotherms for various values of the Rayleigh number and the radiation parameter for a volume fraction of 0.075 are shown in figs. 2–4. In all the Rayleigh numbers analysed, two vortices were created. Considering the boundary conditions and the velocity direction, the streamlines of vortices go up from the vicinity of the middle region of the bottom wall within the enclosure and go down from the side portion of the cold walls. The convection and movement of the nanofluid increase by increasing the Rayleigh number. It is observed that, in the region where the two vortices are near to one another, the density of the streamlines is higher. A higher density of streamlines shows a higher speed of the hybrid nanofluid in the region. As is seen from fig. 2 and fig. 3, the streamlines for $Ra = 10^3$ and $Ra = 10^4$ are similar to each other.

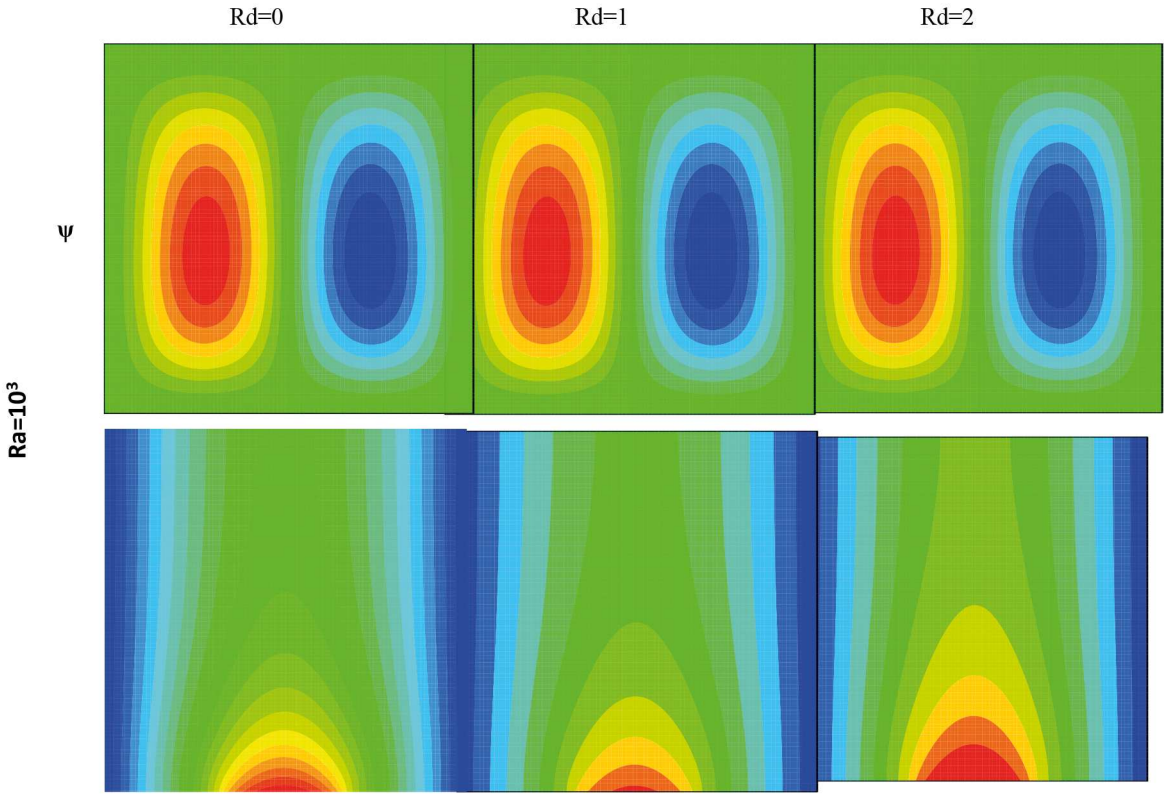

Fig. 2. Streamlines and isotherms for $Ra = 10^3$ and different values of the radiation parameter, $\varphi = 0.075$.

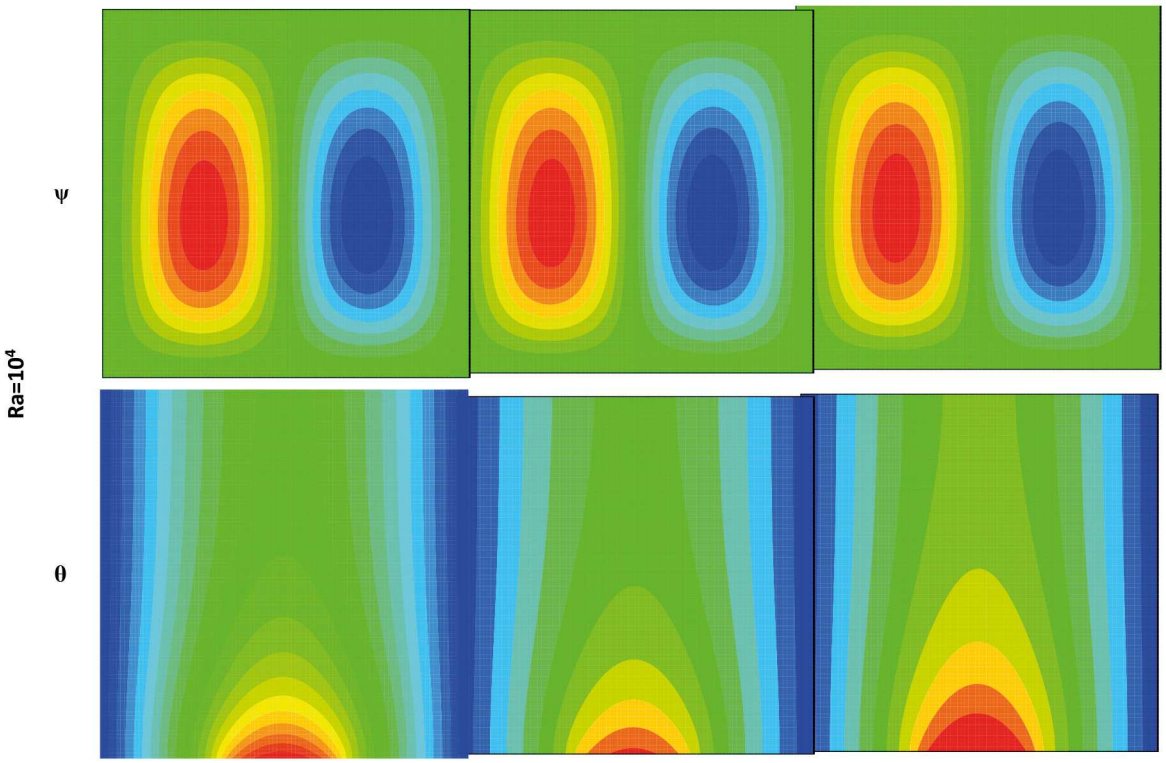

Fig. 3. Streamlines and isotherms for $Ra = 10^4$ and different values of the radiation parameter, $\varphi = 0.075$.

The amount of isotherms in the vicinity of the bottom wall is higher than in the other region within the enclosure. Also, the density of isotherms in this region is higher in comparison to the other regions and this is a sign of a higher heat transfer rate in this region. On the basis of the results shown in fig. 3, the heat penetration (or development) in the middle portion of the enclosure is higher than that on the sides of the vertical walls. As is seen in the figures, the

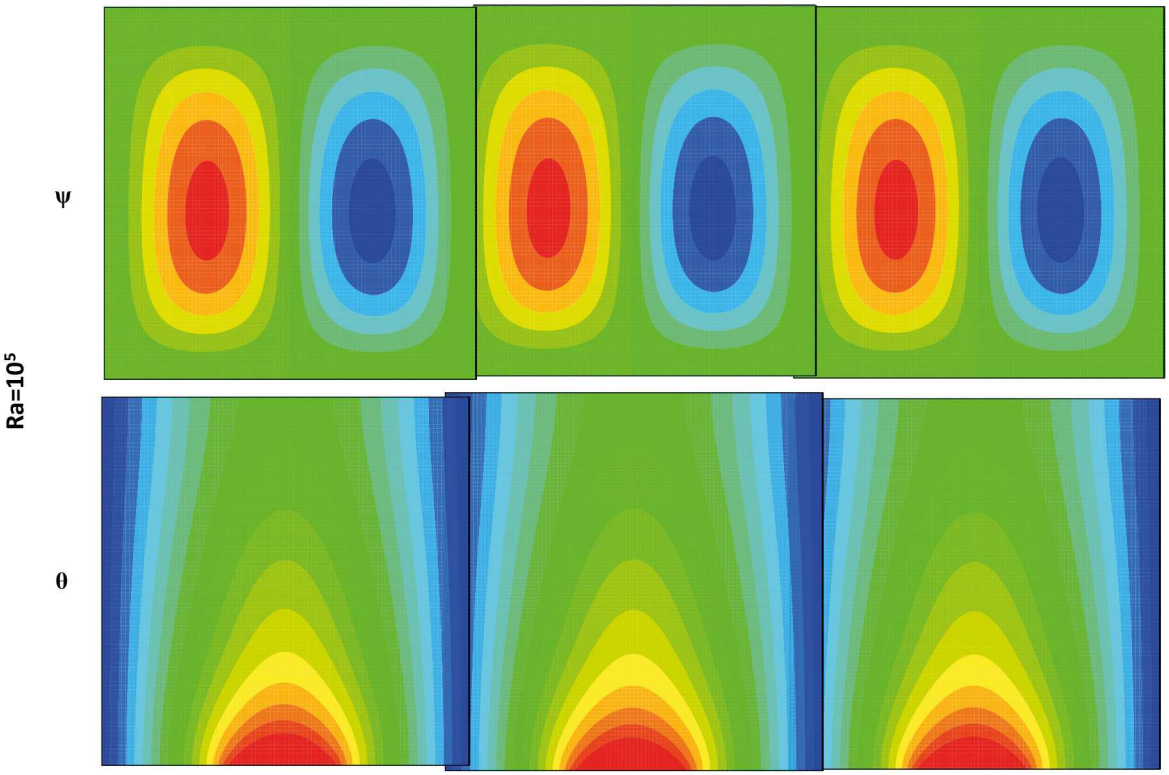

Fig. 4. Streamlines and isotherms for $Ra = 10^5$ and different values of the radiation parameter, $\varphi = 0.075$.

density of the isotherms in the vicinity of the vertical walls within the enclosure for $Ra = 10^5$ is higher in comparison to lower Rayleigh numbers. This behaviour of isotherms is caused by the decrease in the thickness of the thermal boundary layer as a result of increasing the buoyancy force which increases by increasing the Rayleigh number.

For $Ra = 10^3$ and $Ra = 10^4$, the heat penetration increases by increasing the radiation parameter and the region in the vicinity of the bottom walls has a higher temperature. For $Ra = 10^5$ and a radiation parameter of 0.1 in comparison to a lower Rayleigh numbers, the heat penetration is higher but in this ratio of Rayleigh number ($Ra = 10^5$), no alteration is observed in the behaviour of the isotherms which shows that in a high range of Rayleigh numbers the effect of radiation is not significant.

Figure 5 shows the variation of the average Nusselt number with respect to the radiation parameter for different values of Ra and volume fraction of nanoparticles. For all volume fraction values investigated, the average Nusselt number increases by increasing the radiation parameter. The heat transfer within the enclosure increases more as a result of increasing the radiation parameter to higher values; and this yields higher values of the average Nusselt number. In all of the considered values for Ra and volume fraction, the relevant enhancement in the average Nusselt number is obtained due to increasing the radiation parameter is 200.25 percent ($Ra = 10^5$, volume fraction = 0.075). There is no appreciative change in the average Nusselt number for $Ra = 10^3$ and $Ra = 10^4$ employed in all volume fractions and radiation parameters considered. Actually, the enhancement of the Rayleigh number is not enough to make an appreciative change in the rate of the heat transfer but it is worth noticing that the average Nusselt number decreases when the Rayleigh number increase to 10^6.

An increase in the nanofluid movement within the enclosure acts as an obstacle for a better radiation heat transfer and yields a decrease in the average Nusselt number. Thus, it is not effective to apply radiation for the purpose of heat transfer enhancement in the high Rayleigh number investigated in this study.

Considering all radiation parameters for each Rayleigh number investigated, the average Nusselt number increases by increasing the volume fraction. The maximum enhancement of the average Nusselt number with respect to increasing the volume fraction of nanoparticles is 8.37 percent which occurs for $Ra = 10^3$, while the volume fraction of nanoparticles is varied from 0.0 to 0.075.

Figure 6 shows the variation of the maximum value of the stream function with respect to the radiation parameter for various values of the Rayleigh number and the volume fraction of nanoparticles. For all values of the volume fraction investigated, the maximum value of the stream function increases by increasing the value of the radiation parameter. Enhancement of heat transfer by increasing the radiation parameter is due to enhancement of the buoyancy force which increases the movement of nanoparticles within the enclosure. Increasing the movement and convection of the

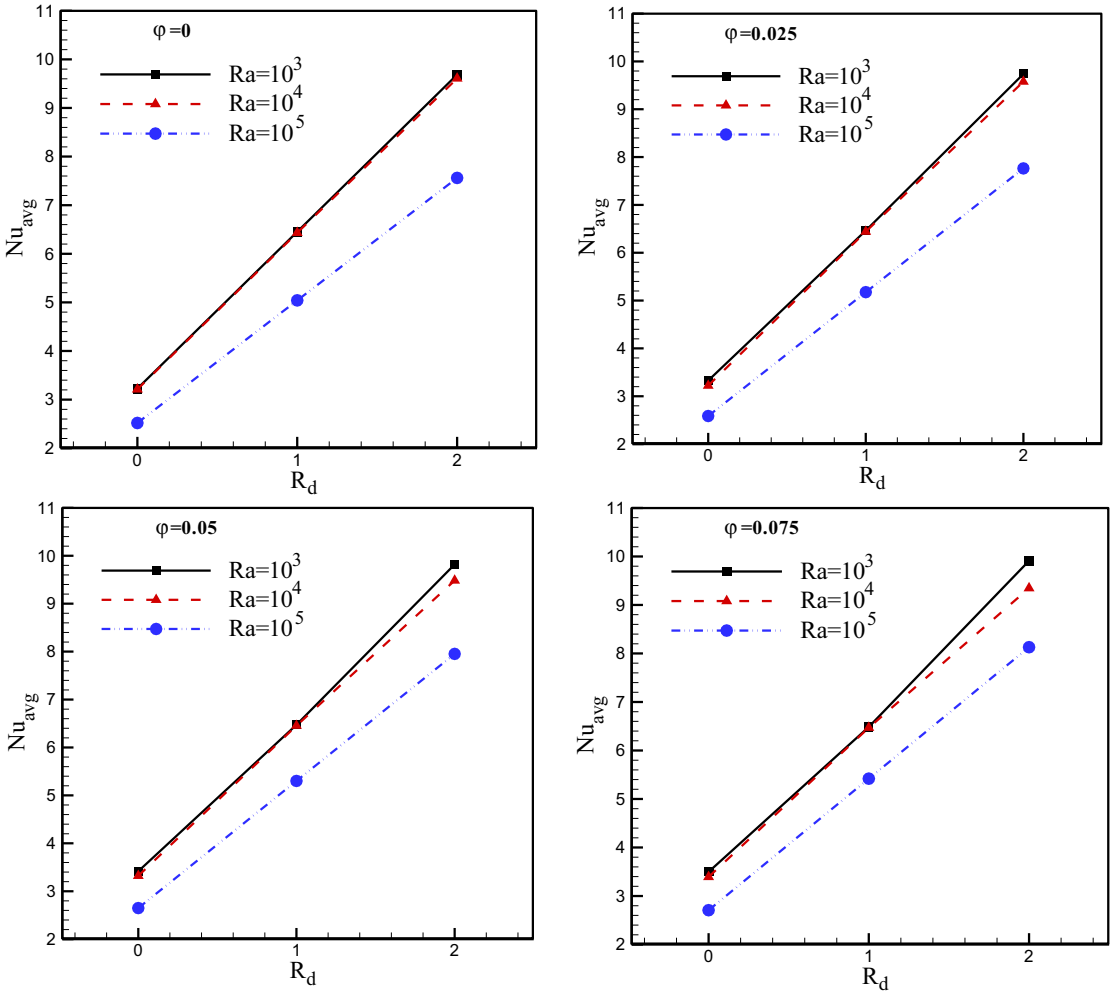

Fig. 5. Variation of average Nusselt number with respect to R_d for different values, of Ra and φ.

nanofluid within the enclosure causes an enhancement in the maximum value of the stream function as a sign of the power criteria of the fluid flow. The highest enhancement in the maximum value of the stream function as a result of the R_d (radiation parameter) enhancement is measured to be 11.49 percent which is caused by all Rayleigh numbers and volume fraction investigated, which occurs for $Ra = 10^5$ while the volume fraction of nanoparticles is 0.075.

For all Rayleigh numbers for each value of the radiation parameter investigated, the maximum value of the stream function decreases by increasing the volume fraction of nanoparticles; and all these are raised by increasing the friction (depending on viscosity) which resulted from the volume fraction enhancement caused by increasing the viscosity of the nanofluid. Considering all the radiation parameters for each Rayleigh number investigated, the maximum value of the stream function increases by increasing the volume fraction; and the highest reduction in the maximum value of the stream function as a result of increasing the volume fraction of nanoparticles is 24.72 percent which occurs for $Ra = 10^5$ while the volume fraction of nanoparticles is varied from 0.0 to 0.075.

7 Conclusion

In this study, the impact of thermal radiation on fluid flow and heat transfer within a square enclosure filled with ethylene glycol-Co_3O_4-diamond hybrid nanofluid on the basis of experimental data, is investigated. This study focuses on $Ra = 10^3$ to $Ra = 10^5$ and the volume fraction of nanoparticles in the range from 0.0 to 0.075 percentage and 0 to 2 for radiation parameter. The following conclusions are observed from the results:

- In all volume fractions investigated, the average Nusselt number increases by increasing the radiation parameter.
- In all of the considered values for Ra and the volume fraction, the highest enhancement in the average Nusselt number as a result of increasing the radiation parameter is 200.25 percent which occurs for $Ra = 10^5$ while the volume fraction is 0.075.

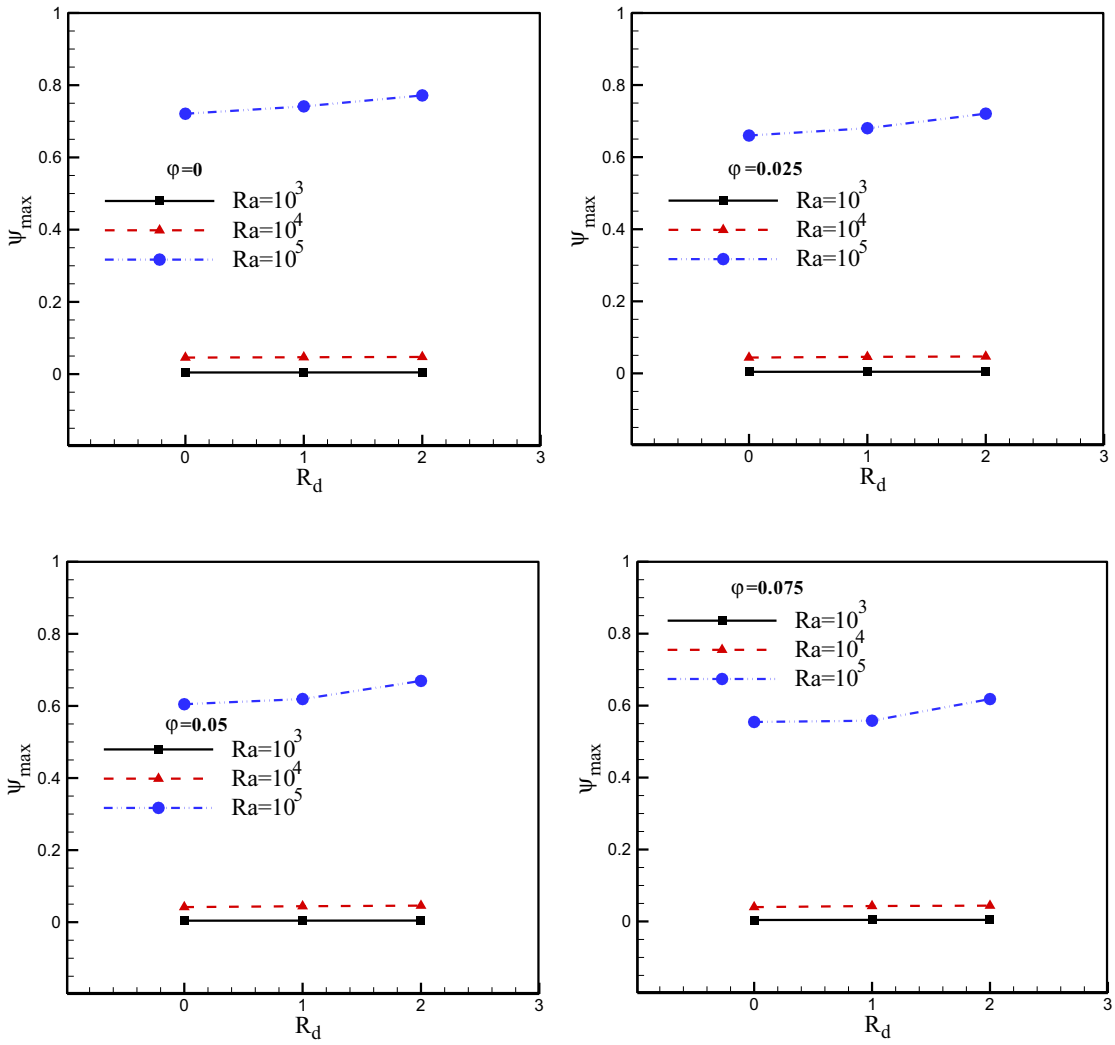

Fig. 6. Variation of the maximum value of the stream function respect to R_d for variable Ra and φ.

- There is no significant change in the average Nusselt number for $Ra = 10^3$ and $Ra = 10^4$ employed in all considered values of the volume fraction and the radiation parameter.
- Considering all radiation parameters for each Rayleigh number investigated, the average Nusselt number increases by increasing the volume fraction. The maximum enhancement of the average Nusselt number with respect to increasing the volume fraction of nanoparticles is 8.37 percent which occurs for $Ra = 10^3$, while the volume fraction of nanoparticles is varied from 0.0 to 0.075.
- In all volume fractions investigated, the maximum value of the stream function is increased by increasing the value of the radiation parameter.
- The highest enhancement in the maximum value of the stream function as a result of the R_d (radiation parameter) enhancement is measured to be 11.49 percent which is obtained from all Rayleigh numbers and volume fraction investigated which occurs for $Ra = 10^5$ while the volume fraction of nanoparticles is 0.075.
- For all Rayleigh numbers and each radiation parameter investigated, the maximum value of the stream function decreases by increasing the volume fraction of nanoparticles.
- Considering all radiation parameters for each Rayleigh number investigated, the maximum value of the stream function increases by increasing the volume fraction.
- The most relevant reduction in the maximum value of the stream function as a result of increasing the volume fraction of nanoparticles is 24.72 percent which occurs for $Ra = 10^5$ while the volume fraction of nanoparticles is varied from 0.0 to 0.075.

Nomenclature

c_P	Specific heat at constant pressure (J kg^{-1} K^{-1})	β	Coefficient of thermal expansion (K^{-1})
g	Gravitational acceleration (m s^{-2})	μ	Viscosity (kg m^{-2} s^{-1})
Ra	Rayleigh number	υ	Kinematic viscosity (m^2 s^{-1})
L	Enclosure height (m)	Θ	Dimensionless temperature
k	Coefficient of thermal conductivity (W m^{-1} K^{-1})	ρ	Density (kg m^{-3})
Nu_{avg}	Average Nusselt number	φ	Volume fraction of nanoparticles
P	Pressure (Pa)	ψ	Stream function (m^2 s^{-1})
Pr	Prandtl number	**Footnotes**	
R_d	Radiation parameter	avg	Average
T	Temperature (K)	c	Cold
u	Velocity component in the x-direction	f	Fluid
v	Velocity component in the y-direction	h	Hot
U	Dimensionless velocity component in the x-direction	nf	Nanofluid
V	Dimensionless velocity component in the y-direction	max	Maximum
Greek symbols			
α	Thermal diffusivity (m^2 s^{-1})		

References

1. K. Khanafer, K. Vafai, M. Lightstone, Int. J. Heat Mass Transfer **46**, 3639 (2003).
2. C.J. Ho, M.W. Chen, Z.W. Li, Int. J. Heat Mass Transfer **51**, 4506 (2008).
3. H. Oztop, E. Abu-Nada, Int. J. Heat Fluid Flow **29**, 1326 (2008).
4. E.B. Öğüt, Int. J. Thermal Sci. **48**, 2063 (2009).
5. M. Jahanshahi, S.F. Hosseinizadeh, M. Alipanah, A. Dehghani, G.R. Vakilinejad, Int. Commun. Heat Mass Transfer **37**, 687 (2010).
6. H. Saleh, R. Roslan, I. Hashim, Int. J. Thermal Sci. **54**, 194 (2011).
7. S.M. Aminossadati, B. Ghasemi, Int. Commun. Heat Mass Transfer **38**, 672 (2011).
8. M. Mahmoodi, S.S. Hashemi, Int. J. Therm. Sci. **55**, 76 (2012).
9. P. Valipour, R. Moradi, F. Shaker Aski, J. Mol. Liq. **237**, 242 (2017).
10. M. Hassan, C. Fetecaub, A. Majeed, A. Zeeshan, J. Magn. & Magn. Mater. **465**, 531 (2018).
11. M. Sheikholeslami, A. Zeeshan, A. Majeed, J. Mol. Liq. **268**, 354 (2018).
12. N. Shehzad, A. Zeeshan, R. Ellahi, Commun. Theor. Phys. **69**, 655 (2018).
13. Farooq Hussain, Rahmat Ellahi, Ahmad Zeeshan, Appl. Sci. **8**, 275 (2018).
14. A. Zeeshan, N. Shehzad, R. Ellahi, Results Phys. **8**, 502 (2018).
15. M. Sheikholeslami, A. Zeeshan, Int. J. Numer. Methods Heat Fluid Flow **28**, 641 (2017).
16. A.S. Dogonchi, D.D. Ganji, J. Taiwan Inst. Chem. Eng. **80**, 52 (2017).
17. L.S. Sundar, J. Hortiguela, K. Singh, C. Sousa, Int. Commun. Heat Mass Transfer **76**, 245 (2016).
18. G.A. Sheikhzadeh, H. Khorasanizadeh, S.P. Ghaffari, Trans. Phenom. Nano Micro Scales **1**, 75 (2013).
19. M. Sheikholeslami, T. Hayat, A. Alsaedi, Int. J. Heat Mass Transfer **96**, 513 (2016).
20. L. Syam Sundar, G.O. Irurueta, E. Venkata Ramana, Manoj K. Singh, A.C.M. Sousa, Case Studies Therm. Eng. **7**, 66 (2016).
21. M. Afrand, Int. J. Therm. Sci. **118**, 12 (2017).
22. M. Afrand, S. Farahat, A.H. Nezhad, G. Ali Sheikhzadeh, F. Sarhaddi, Int. J. Appl. Electromagn. Mech. **46**, 809 (2014).
23. M. Afrand, S. Farahat, A.H. Nezhad, G.A. Sheikhzadeh, F. Sarhaddi, Heat Transfer Res. **45**, 749 (2014).
24. M. Afrand, S. Farahat, A.H. Nezhad, G.A. Sheikhzadeh, F. Sarhaddi, S. Wongwises, Int. Commun. Heat Mass Transfer **60**, 13 (2015).
25. M. Afrand, S. Rostami, M. Akbari, S. Wongwises, M.H. Esfe, A. Karimipour, Int. J. Heat Mass Transfer **90**, 418 (2015).
26. M. Afrand, D. Toghraie, A. Karimipour, S. Wongwises, J. Magn. & Magn. Mater. **430**, 22 (2017).
27. M. Mahmoodi, M.H. Esfe, M. Akbari, A. Karimipour, M. Afrand, Int. J. Appl. Electromagn. Mech. **47**, 21 (2015).
28. H. Teimouri, M. Afrand, N. Sina, A. Karimipour, A.H.M. Isfahani, Int. J. Appl. Electromagn. Mech. **49**, 453 (2015).